Electrical Machine Permanent Magnets Health Monitoring and Diagnosis Using an Air-Gap Magnetic Sensor

Anees Mohammed, Juan I. Melecio, and Siniša Djurović, *Member, IEEE*

***Abstract*—this study proposes a magnetic sensor design and application for monitoring the health of rotor magnets in permanent magnet (PM) electrical machines through in-situ observation of the air-gap magnetic flux density. The reported device employs the concept of Fibre Bragg Grating (FBG) strain sensing fusion with magnetostrictive material to deliver a machine stator slot wedge integrated sensor that allows straightforward installation and retrofit with no invasive action to core elements of the machine. The sensing theory, design, prototyping, calibration and installation of the proposed magnetic sensing scheme are detailed in the paper. The sensor was installed into an inverter driven surface mount PM synchronous machine (SPMSM) and its performance for in-situ observation of rotor PM magnetization conditions validated in a range of healthy and demagnetised PM conditions tests. The obtained experimental data demonstrate the reported device's capability to enable recognition of rotor PMs' magnetisation level and thus their health monitoring. Finally, a fault index is proposed and experimentally validated that allows the application of in-situ magnetic sensor measurements for relative quantification of PM demagnetization fault severity.**

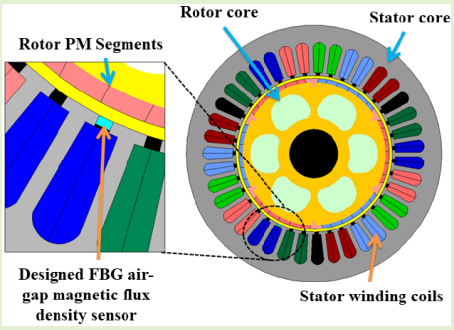

***Index Terms*— PM machines, magnetic sensing, demagnetisation diagnosis, FBG strain sensor, magnetostriction.**

I. Introduction

PERMANENT magnet (PM) machines are key elements of a number of contemporary industrial systems, ranging from application as preferred propulsion motor choice in modern electric vehicles to being enabling components of military, medical, factory automation, aerospace and wind energy systems [1], [2]. A large proportion of PM machines applications in these areas is operationally and/or safety critical. The capability of reliable monitoring and timely diagnosis of PM machine faults has thus become an important requirement for effective utilisation of these systems [1]–[3].

Magnet demagnetisation is a common and key failure mode in PM machines [3]. PM demagnetisation is critical since it invariably causes machine performance degradation and can lead to complete machine failure and loss of functionality. Demagnetisation can be caused by high operating temperature or a demagnetising magnetic field [4]; in addition, mechanical and environmental stresses can result in PM mechanical damage, i.e. chipped, cracked or corroded magnets, which can alter their magnetization characteristic [4]. PM demagnetisation faults are generally classified as local or uniform depending on the location and distribution of the demagnetisation area [5].

Development of new techniques for PM health condition monitoring in electrical machines and diagnosis of their magnetisation condition is receiving a growing interest [3]–[9]. The reported monitoring techniques largely focus on exploring non-invasive methods, with invasive methods being less researched. The non-invasive techniques are largely based on electric and electromagnetic signals monitoring such as current, voltage, Back Electromotive Force (back EMF) or magnetic flux [4]–[6]; these techniques have shown considerable limitations in delivering reliable diagnosis due to the challenge of identifying dependable fault signature. To overcome this, application of advanced artificial intelligence methods, such as neural networks, was proposed [3], [7]; these can however suffer from diagnostic unreliability and require large data sets for training. Invasive techniques application, such as search coil [8] and vibration [9] sensor usage were explored for PM faults diagnosis. While

Manuscript received November 2, 2019; revised January 16, 2020; accepted January 16, 2020. Date of publication January 27, 2020; date of current version April 16, 2020. This work was supported by the U.K. Engineering and Physical Sciences Research Council (EPSRC) HOME-Offshore through the Holistic Operation and Maintenance for Energy from Offshore Wind Farms Consortium under Grant EP/P009743/1. The associate editor coordinating the review of this article and approving it for publication was Dr. Anuj K. Sharma. *(Corresponding author: Siniša Djurović.)*

The authors are with the School of Electrical and Electronic Engineering, The University of Manchester, Manchester M13 9PL, U.K. (e-mail: anees.mohammed@manchester.ac.uk; ignacio.melecio@manchester.ac.uk; sinisa.durovic@manchester.ac.uk).

Digital Object Identifier 10.1109/JSEN.2020.2969362

of interest these methods can have limitations in diagnostic capability or suffer from measurement errors and practical application challenges due to installation complexity.

Fibre optic sensing has emerged as a promising alternative for electric machine condition monitoring: its application for machine mechanical and thermal monitoring [2], [10]–[13] is attracting increased interest. The FBG sensing technology, with its advanced features such as small size, Electromagnetic Interference Immune (EMI), multiplexing and multi-physical sensing presents a promising proposition for enabling targeted in-situ monitoring of machine multi physical operating conditions. FBG magnetic sensing applications for electrical machine monitoring are only starting to be examined, with very recent reports suggesting encouraging potential for this application in non-permanent magnet machines (induction machine and hydro generator) but not exploring PM machine applications [14]–[16]. Furthermore, the application of reported magnetic sensing methods to a wider range of electrical machines would be practically limited, due to their design imposing either requirements for invasive installation methods, or limitations on the sensor integration within an arbitrary test machine geometry.

This paper proposes a magnetic sensing device design and application for in-situ monitoring of the air-gap flux density to enable health diagnosis of PMs in rotating electrical machines. The reported sensor is based on integration of FBG strain sensing technology with a highly magnetostrictive material (Terfenol-D) [17] in a simple geometry that is small in size and enables straightforward installation and retrofit in existing machinery. The sensor is in this application installed as part of a stator slot wedge, thus enabling effective monitoring of entire rotor PM material volume and crucially a flexible and straightforward installation procedure that does not compromise the integrity of core machine elements. The proposed magnetic sensor design, prototyping, calibration and installation procedures are detailed in the paper. The sensor was installed in a purpose built permanent magnet synchronous machine (SPMSM) and its performance in monitoring rotor PMs' health status examined in a range of experiments, involving operation with and without PM demagnetisation fault. The used laboratory test system is specially developed to enable practical emulation of SPMSM PM demagnetisation conditions through replacement of the healthy rotor with identical rotor geometries having predefined in-built levels of uniform PM demagnetization. The presented experimental results demonstrate that the proposed scheme enables recognition of the existing PM magnetisation state and its change with the demagnetisation fault presence within the machine nominal operating range: the proposed sensor clearly registers the rotating magnetic field produced by the rotor magnets. Finally, a diagnostic index defined by processing the distinct in-situ magnetic measurement features is proposed that enables relative quantification of the existing demagnetization fault severity.

II. In-Situ Magnetic Sensor Design

The core functionality of the magnetic sensor proposed in this study is based on combining the FBG inherent strain sensing feature with high magnetostriction properties of Terfenol-D material [16], [17]. The following sub-sections present the details of the sensor design, prototyping and calibration procedures.

A. FBG Strain Sensing Principles

An FBG sensor is a small structure, typically a few millimeters in length, imprinted in a core of a single-mode optical fiber [18]. An FBG is fabricated by exposure of the fiber core section where the sensing head needs to be placed to an interference pattern of Ultraviolet light, which induces a permanent periodic change (i.e. gratings) in the fiber core's refractive index [10]. In principle, an FBG sensor operates as a light filter that reflects a narrowband light wavelength when a fiber carrying it is illuminated by a broad band light source. The FBG reflected light wavelength is known as the Bragg wavelength, λ_{B}, and is defined as [2]:

$$\lambda_B = 2\Lambda n_{eff}, \tag{1}$$

where: Λ is the grating period and n_{eff} is the effective refractive index. These parameters alter with the variation in the temperature and strain imposed on the FBG structure, thus altering the reflected narrowband wavelength. Assuming a constant temperature, the variation in λ_{B} due to strain variation $\Delta\varepsilon$ can be expressed as [10]:

$$\frac{\Delta\lambda_B}{\lambda_B} = 2\left(\Lambda\frac{dn_{eff}}{d\varepsilon} + n_{eff}\frac{d\Lambda}{d\varepsilon}\right)\Delta\varepsilon \tag{2}$$

The response of the FBG sensor to strain arises due to the change in the grating period (due to the physical elongation of the sensor), and the change in the reflective index due to photo-elastic effects. A typical theoretical value of strain sensitivity for a standard FBG sensor imprinted with λ_B at 1500 nm is $\approx$ 1.2 pm/μ strain. This value, however, can vary depending on the FBG sensor packaging and installation methods [11]. In the magnetic sensor design reported in this work the FBG strain sensing capability is used to observe the geometry deformation in a plate of highly magnetostrictive Terfenol-D when exposed to a rotating PM field.

B. Terfenol-D Magnetostrictive Features

Magnetostriction is an effect that causes a change in the shape of a ferromagnetic material when subjected to a magnetic field. In principle, external magnetic fields cause inherent internal strains in magnetostrictive materials that result in their dimension change largely along the magnetic field direction. The magnetostrictive effects are generally classified as [19], [20]: Joule (longitudinal only extension), volume (volumetric expansion), Wiedemann (twisting due to helical magnetic field) and form (magnetostatic effect). The magnetostrictive volume effect, which is the volumetric change in presence of magnetic field is used in the sensor design reported in this study.

Terfenol-D (Terbum *Ter*, Iron *Fe*, Naval Ordnance Laboratory *NOL*, Dysposrium *D*) is among ferromagnetic materials exhibiting the largest known levels magnetostrictive expansion at room temperature [21], [22]. It is currently commercially available in a variety of different forms, including thin

slices, powder composites and monolith solid samples [22]. When exposed to a magnetic field, Terfenol-D can produce magnetostrictive extension (strain) in the reported range of 800−1200 parts per million (ppm), which makes it a strong candidate for magnetic sensing applications [22].

Terfenol-D magnetostriction characteristics are a unipolar phenomenon, independent of the magnetic field direction, meaning that either a contraction or an extension is produced in the presence of positive and negative magnetic fields. Additionally, the strain output of Terfenol-D is highly non-linear (butterfly shape hysteresis curve) and while it is generally approximately proportional to the square of the magnetic field it is also highly dependent on the mechanical pre-stress level applied to the alloy [19].

C. FBG-Magnetostrictive Sensor Design and Prototyping

The target sensing application in this study is the in-situ monitoring of PMs' health condition in in-service PM electrical machines. To this end, the reported magnetic sensor design employs FBG strain sensing capability bonded to an appropriately dimensioned Terfenol-D plate to observe its geometry deformation when exposed to a rotating PM field within the machine air-gap.

To ensure optimal sensor performance while delivering a minimally invasive and fully retrofittable monitoring capability the sensor is designed to be integrated within a modified stator slot wedge structure: this allows for effective exposure of the Terfenol–D plate to the rotating PM radial field, while minimally interfering with the main flux paths into the stator teeth and requiring no physical disturbance to the machine magnetic circuit or structure. Furthermore, to simplify the sensor application and allow for a more practical design while retaining sensing functionality, a Terfenol-D plate directed axially, lengthwise along the slot wedge structure and with its anisotropy axis perpendicular to the observed PM field, is used [16]. This ensures the magnetic sensor is located as close as possible to the rotor magnets. It also allows the sensor to be fixed in a stationary stator position and thus be readily capable of observing the field produced by all passing rotor PMs. Finally, this imposes no requirement for invasive action to main elements of the machine magnetic or electrical circuit during sensor installation, and enables relatively straightforward installation and retrofit procedures.

Based on the above principles this study designs a magnetic-sensor to be applied in a commercial SPMSM test motor, detailed in section III. Fig.1 illustrates the architecture of the developed sensor. A Terfenol-D piece (TdVib LLC, USA) of rectangular prism geometry with dimensions of 10 mm (length) x 1.62 mm (width) x 1 mm (height) is used, illustrated in Fig. 1a [19]. The Terfenol-D plate was dimensioned to enable installation into the stator slot opening geometry of the examined SPMSM. This was done by bonding the plate to a specially designed slot wedge retrofitted to the test motor.

For flexibility and optimal performance and installation, the retrofitted wedge that houses the magnetic sensor is

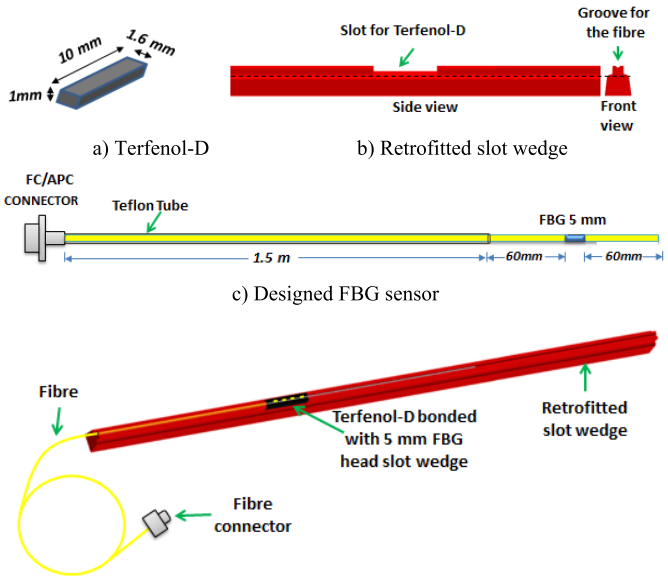

Fig. 1. In-situ flux sensitive device design and prototyping architecture.

manufactured from a rapid prototyping (RP) plastic material (ABSplus-P430 by Stratasys©), which has sufficient strength to withstand the mechanical assembly process involving insertion into a stator slot, and to resist the attractive magnetic forces produced by the PM rotor on the sensor assembly. The slot wedge was fabricated using a Dimension 1200es RP machine by Stratasys©which uses the Fused Deposition Modelling (FDM) technology [23]. The 3D printed wedge architecture was designed to enable seamless integration of the magnetic sensor into its structure, as shown in Fig. 1b: its geometry is designed to contain an upper structure with a single fine groove on top to be located within the stator slot opening; in addition, a suitably sized slot has been created in its axial center point to contain the Terfenol-D plate. This resulting wedge structure allows the location of the magnetostrictive plate in a desired position at the air-gap, ensuring its effective exposure to the flux produced by the passing rotor PMs; the designed fine groove enables straightforward installation of a sensing fibre carrying an FBG head to be bonded to the fixed Terfenol-D plate.

An FBG sensor with a 5 mm FBG head imprinted in polyamide single-mode optical fibre was designed and prototyped, see Fig. 1c. The FBG head was bonded to the top centre point (facing the machine air-gap) of the Terfenol-D plate using a commercial cyanoacrylate glue (Loctite©Super Glue): in this position the formed FBG-magnetostrictive magnetic sensor is directly exposed to the rotating PM excitation. The installed fibre was housed in the slot wedge groove and its remainder packaged in a Teflon tube to provide adequate mechanical protection and routed outside the test motor to the interrogator, as illustrated in Fig. 1d.

D. Sensor Calibration

To ensure the developed magnetic sensor's response represents the measured magnetic flux density on a credible scale the sensor was calibrated on a purpose built laboratory

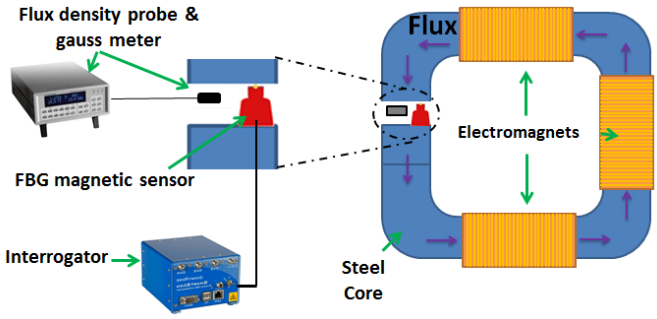

Fig. 2. Calibration test-rig setup.

TABLE I
FBG-TERFENOL-D SENSOR RESPONSE DURING STATIC CALIBRATION TESTS

Current (A)	2.5	5	7.5	10	12.5	15	17.5	20	22.5	25
Flux density meter (T)	0.155	0.304	0.448	0.575	0.690	0.794	0.883	0.953	0.996	0.984
FBG sensor (nm)	0.072	0.205	0.366	0.47	0.534	0.563	0.57	0.577	0.582	0.582

system illustrated in Fig. 2. The system comprises a C shaped magnetic core containing electromagnets with controllable excitation, allowing the desired set magnetic flux density conditions to be established in its air-gap. The rig also contains a commercial Lake Shore Cryotronics MNT-4E04-VG flux density probe installed in the air-gap: this enables the tested magnetic sensor response (i.e. wavelength shift at a known flux density level) calibration against a reliable reference.

During calibration tests the FBG-magnetostrictive sensor and the commercial probe were located in very close proximity within the test core air-gap. Both the test and the reference sensor were then activated and the magnetic core energized to provide the air-gap magnetic field; the FBG sensor is operated by a SmartFibres SmartScan04 interrogator unit while the flux meter is run using a Lake Shore Cryotronics 460 3-CH Gaussmeter unit. The C-core electromagnets were energized in a series of DC current levels in steps of 2.5 A to induce a number of distinct points in a magnetic flux density variation range representative of that encountered in a commercial PMSM air-gap (i.e. <1T).

Table I shows the corresponding wavelength shifts measured by the magnetic sensor and the flux densities recorded by the commercial probe: the magnetic sensor is seen to have observed wavelength shifts of up to 0.580 nm due to Terfenol-D magnetostriction induced strain through exposure to test flux density of up to 0.98 T. The obtained calibration data were used to calculate the appropriate wavelength shift-magnetic flux fit curve for the magnetic sensor. Plots of the original calibration test data along with the calculated fit curve are shown in Fig. 3; a 5th order polynomial fit curve was used and is shown in the figure for completeness. The effect of temperature variation on the FBG magnetic sensor measurements is not fully demonstrated in this work which focuses on examining the proposed sensor's diagnostic performance in representative steady-state thermal conditions. The rate of variation of thermal conditions in a PM machine is intrinsically much lower than the air-gap field variation rates and thus thermal variation is not expected to have a detrimental

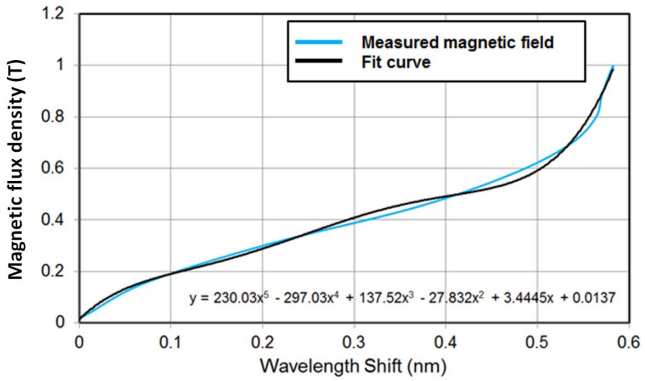

Fig. 3. Measured wavelength shift vs applied flux.

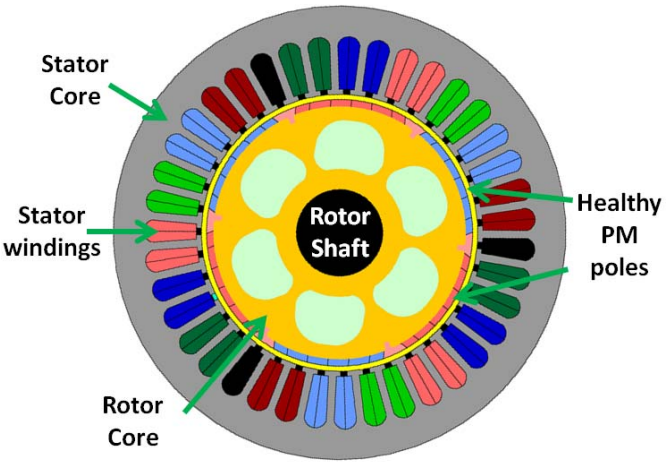

Fig. 4. Cross-sectional view of the examined SPMSM geometry.

effect on the relevant in-situ field measurements and therefore the diagnostic performance of the proposed technique.

III. EXPERIMENTAL SYSTEM SETUP

The proposed magnetic sensor was fitted into a test SPMSM that enables experimental emulation of a range of healthy and demagnetized rotor PM conditions. The following sub-sections describe the sensor installation procedure, the experimentally examined rotor PM magnetic conditions and the general test rig design and operational features.

A. Flux Sensor Embedded SPMSM

The examined motor is a three-phase, 6 pole, 1.1kW, 415V, 90Hz, surface mounted PM (SPM) design manufactured by Lafert motors. The stator has a concentric winding configuration with 6 coils per phase connected in series. The rotor is a non-skewed SPM design containing arc-shaped N-35 grade Neodymium PMs with a pitch of 147° ($\propto_e$). For the purpose of this study each PM pole arc was remanufactured/refitted to be circumferentially segmented into six individual sections. The cross section of the test SPMSM is shown in Fig. 4.

The slot wedge integrated magnetic sensor design detailed in section II. C was fitted in one of stator slots of the test motor, as illustrated in Fig. 5. The top surface of the Terfenol-D plate where the FBG sensing head is bonded is kept level

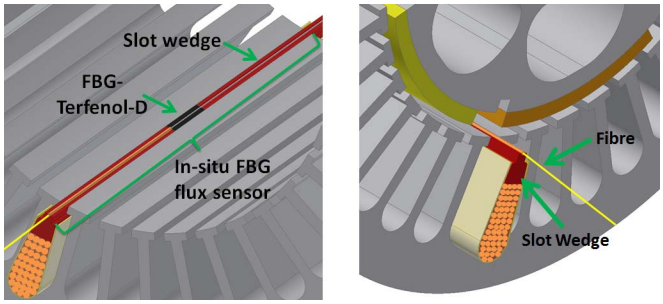

Fig. 5. FBG magnetic flux sensor embedded slot wedge in the SPMSM.

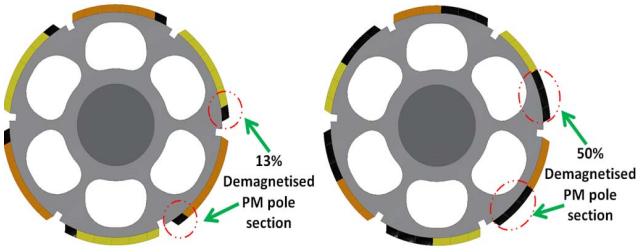

a) Rotor 1: 13% Demag b) Rotor 2: 50 % Demag

Fig. 6. Test rotors with uniform demagnetization fault.

in this process with the stator inner bore to ensure effective sensor exposure to the passing rotor PMs fields. The sensor is installed in a stator slot of arbitrary choice, as the selection of its slot position does not affect its performance.

B. The Examined Demagnetised Rotor Conditions

The in-service performance of the in-situ magnetic sensor was tested in experiments on the test motor operating with a healthy rotor and with purpose built rotors with uniform demagnetization faults; the uniform demagnetisation faults are manifested as identical modulation of the PM segments flux density, B_r, under each pole [24]. In addition to the healthy rotor, two faulted test rotors were built to enable the emulation of two different levels of uniform de-magnetisation conditions. These were of identical geometry to the healthy rotor, however the magnetization state of their PM sections was modified by appropriate application of the individual arc segments following the methodology presented in [25].

Fig. 6 shows the cross section plots of the developed faulted test rotors. Two rotors were designed and built to emulate a 13% (see Fig. 6a) and a 50% (see Fig. 6b) uniform demagnetization condition through B_r reduction at the leading edge of each of the PM pole arcs.

C. Test-Rig Description

The layout of the laboratory test-rig used in this study is shown in Fig. 7. The SPMSM instrumented with the in-situ magnetic sensor was coupled to a 1.1 kW DC load motor to enable testing at desired operating points. The SPMSM was driven by a Parker 890SSD drive operating in Permanent Magnet Alternating Current (PMAC) vector control mode. The FBG sensor was illuminated using a broadband light source provided by a commercial multi-channel interrogator unit. The monitored FBG wavelength was processed using LabVIEW

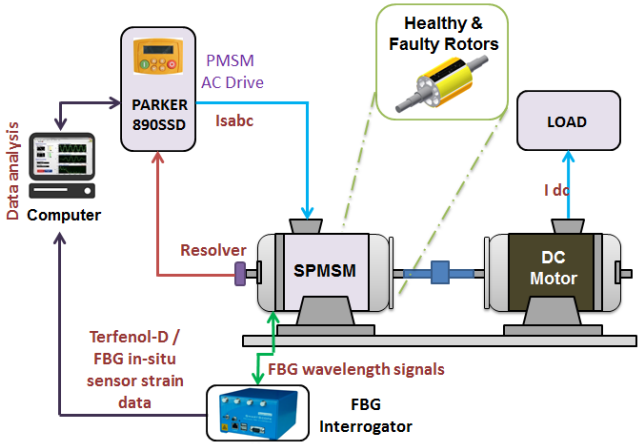

Fig. 7. Test-rig setup.

based SmartSoft software. The SPMSM power, currents and speed were monitored by the drive.

IV. SPMSM Magnetic Field FEA Simulation

The effective interpretation of in-situ magnetic field measurements is in this study underpinned by the understanding of the test motor's air-gap magnetic field distribution under healthy and fault conditions. To this end, an (Finite Element Analysis) FEA model of the examined motor was developed to simulate the motor air-gap magnetic field under healthy and fault conditions, considering the two uniform demagnetization fault cases discussed in section III.B. The FEA model is built using the FLUX2D electromagnetic software package [26]. The two demagnetisation fault scenarios were modeled by setting the magnetic properties of the relevant PM segment sections in each pole to zero. To clearly illustrate the magnetic effects of interest SPMSM operation in the generating regime with the stator windings connected to a resistive load was modelled.

Fig. 8 shows the FEA model results for air-gap flux density versus perimeter distribution for the healthy, 13% demagnetisation and 50% demagnetisation cases, simulated at full speed (FS) and under 25% (see Fig. 8a) and 100% load (see Fig. 8b) conditions for illustration purposes. The presented results demonstrate the effect of the reduction of the active PM arc segment due to the demagnetisation fault, which is seen to lead to redistribution of the air-gap flux density that reflects the loss of active material. In addition, it can be observed in Fig. 8b results that there is an additional increase of the magnetic flux density (see doted circle) in the space corresponding to non-active magnets segments. This field distortion is caused by the flux transition between the opposite poles across the magnetically inactive PM material space and the higher relative permeability of demagnetised PM volume compared to surrounding air; it is observed for all pole transition events in the analysed flux density distribution. At low load conditions however, this effect is not pronounced and is minimal, as evidenced by the data in Fig. 8a. Finally, the effect of stator slotting is clearly manifested as a quasi-regular ripple imposed on the general flux density distribution, as is expected. In a practical application, the observed field distribution

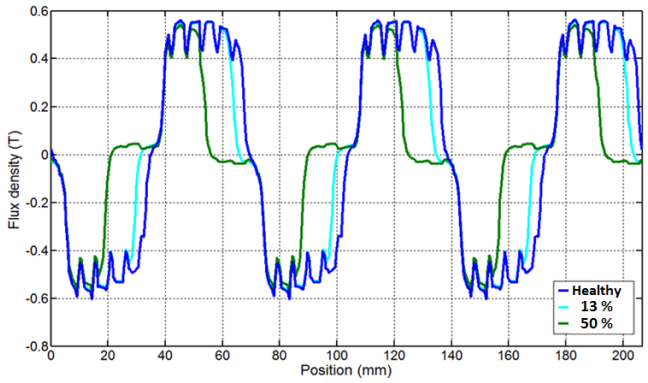

a) Air-gap magnetic flux density at FS and 25 % load

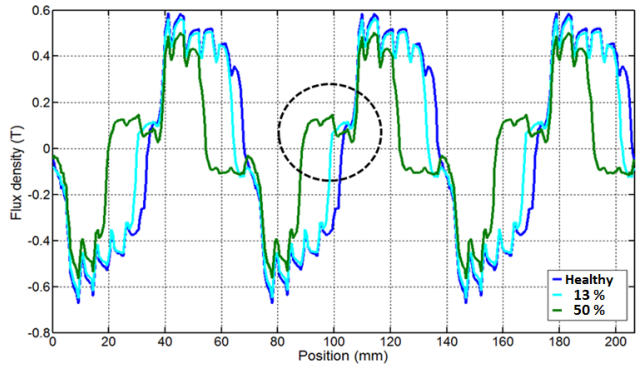

b) Air-gap magnetic flux density at FS and 100% load

Fig. 8. FEA predicted SPMSM air-gap magnetic flux density for healthy, 13% and 50 % demagnetisation conditions.

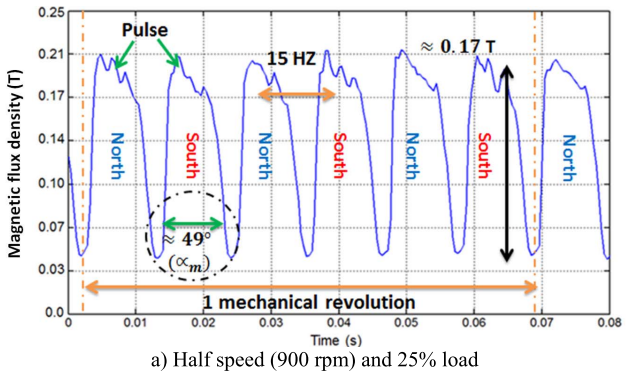

a) Half speed (900 rpm) and 25% load

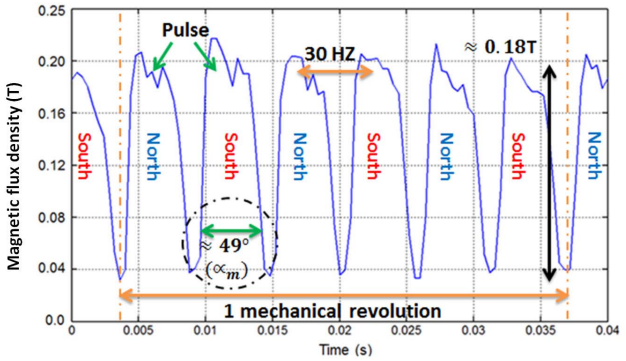

b) Full speed (1800 rpm) and 100% load

Fig. 9. In-situ flux density measurements for a healthy machine.

patterns would be expected to translate into the magnetic sensor Terfenol-D plate magnetostrictive strain variation manifesting a generally consistent variation profile.

V. Experimental Results and Discussion

This section demonstrates and analyses the in-situ in service measurements obtained from the application of the magnetic sensor in different SPMSM operating and health conditions. The section also proposes a diagnostic index for PM health monitoring based on exploiting the features of the in-situ magnetic sensor measurements.

A. Test Procedure and Examined Operating Conditions

The performance of the in-situ sensor was evaluated in tests covering a range of operating speeds and loads within the operating range of the motor, for the healthy and the two demagnetisation fault conditions. Tests were performed for operation at nominal speed (FS, 1800 rpm), 50% of nominal speed (HS, 900 rpm) and 25% of nominal speed (LS, 450 rpm). For each test speed point operation at 100%, 75%, 50% and 25% of nominal load was examined.

The test method applied for each examined healthy and fault case involved running the SPMSM motor at a desired speed using the power electronic drive, and then loading it to the desired point by employing the DC load motor armature current control. To practically emulate demagnetisation faults, the healthy rotor was replaced with one representing the desired fault conditions. The magnetic sensor reflected wavelength was interrogated at a rate of 5 KHz in the tests and then recorded to be post processed in MATLAB.

B. In-Situ Measurements in Healthy Conditions

The baseline performance examination of the in-situ magnetic sensor was performed by analyzing its operation in healthy conditions following the procedure specified in section V.A. For illustration purposes and the sake of brevity the detailed plots of representative measurements are shown in Fig. 9 (HS at 25% load in Fig. 9a and FS at 100% load in Fig. 9b). The healthy machine measurements are seen to report a relatively uniform field variation pattern at a fixed frequency that is rotor speed related (15Hz @ 900rpm and 30Hz @ 1800rpm). The observed pulses in the measurements are an artefact of the deformations induced in the magnetostrictive Terfenol-D piece due to individual rotor magnets' pass events, which are measured as dynamic strain by the FBG head each time a magnet passes the sensor respective position; these strain measurements are converted to magnetic flux density measurement using the magnetic sensor calibration curve.

The Terfenol-D magnetostriction characteristics are independent of magnetic field direction, and thus result in identical polarity pulses measured by the sensor irrespective of the polarity of the rotor PM passing it. The shape of the recorded flux density pulses (pulse width and spacing between pulses) is determined by the SPM rotor design. The pulse width is directly related to the magnets mechanical pitch and is seen to be correctly recorded at $\approx 49°$ mechanical for the examined SPM rotor, while the spacing between adjacent pulses is related to circumferential distance between the adjacent poles (see Fig. 4). The ripple effect due to slotting can also be

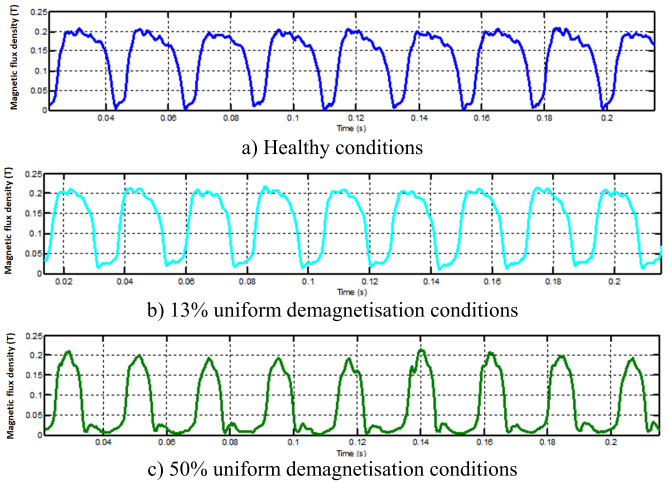

a) Healthy conditions

b) 13% uniform demagnetisation conditions

c) 50% uniform demagnetisation conditions

Fig. 10. In-situ flux density measurements at LS and 25% load.

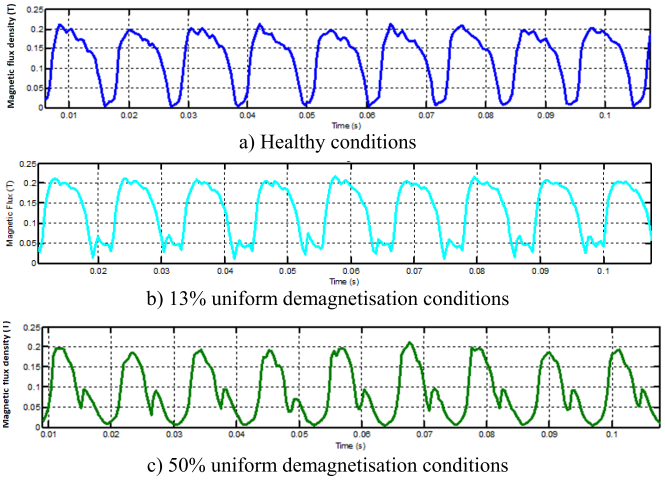

a) Healthy conditions

b) 13% uniform demagnetisation conditions

c) 50% uniform demagnetisation conditions

Fig. 11. In-situ flux density measurements at HS and 50 % load.

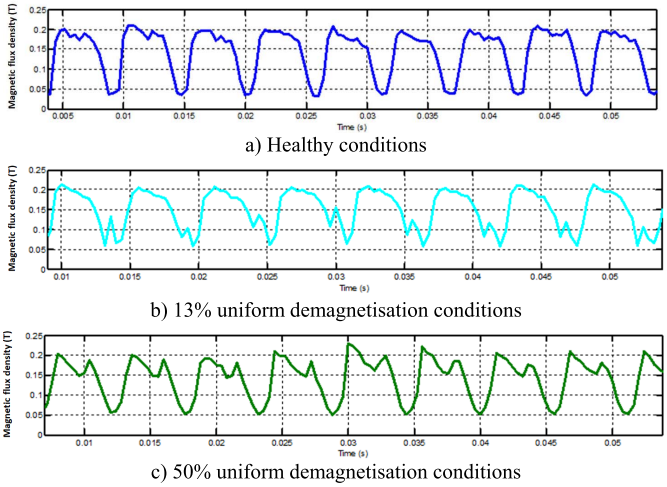

a) Healthy conditions

b) 13% uniform demagnetisation conditions

c) 50% uniform demagnetisation conditions

Fig. 12. In-situ flux density measurements at FS and 100% load.

observed in the obtained measurements, as explained by the simulation results (see fig. 8).

The maximum flux density measurement recorded by the sensor is seen to be $\approx$ 0.18T (pulse peak), which is lower than the simulated air-gap flux density shown in Fig. 8. This is explained by the sensor position in the slot opening: while this location provides an effective, non-invasive sensor placement route, it also means that only a fraction of the PM produced flux will link with the Terfenol-D plate, as the main field path in the machine is through the top of the stator teeth. However the amount of flux captured by the sensor is sufficient to enable monitoring of the rotor PMs' health condition.

The in-situ magnetic sensor has shown a satisfactory response time for registering the rotational magnetic field produced by the rotor magnets for the examined speed conditions. The measurements are seen to enable the determination of rotor mechanical rotational frequency for each examined speed condition. It can be observed that the load has no noticeable effect on the sensor performance and the obtained measurements in healthy conditions.

C. In-Situ Measurements in Demagnetisation Fault Conditions

Sensor performance in PM field observation for faulted rotors was explored for the two fault levels and the same conditions assessed for the healthy machine. The measurements obtained for operation with a healthy, 13% and 50% rotor demagnetisation at LS and 25% load, HS and 50% load, and FS and 100% load are shown in Figs. 10-12.

The measurements in fault conditions are seen to clearly differ in comparison to those in healthy conditions. The measured flux density variation is noticeably different as a result of PM fault field disturbance, with individual pulse widths being particularly affected by the change in PM health conditions. The level of the pulse's magnitude on the other hand exhibits no significant variation; the observed slight magnitude variation is related to the expected minor variation in the peak flux density levels of each test rotor. The pulses' width however is directly related to the active PM arc, as discussed in section V.B, and thus, in demagnetisation fault conditions the measured pulse widths are seen to be clearly reduced, reflecting the field loss induced by the magnet pole arc reduction with fault. Both these effects are in agreement with FEA model predictions in Fig. 8. Furthermore, the measurements are seen to exhibit an increased level of ripple at higher load conditions, which aligns with the patterns observed in section IV FEA model analysis. The obtained measurements clearly demonstrate the capability of the proposed magnetic sensor to register the presence of abnormality in the examined PM rotor.

D. Demagnetisation Severity Diagnosis

The previous sections have demonstrated the in-situ FBG magnetic sensors' capability to enable the recognition of general rotor PM demagnetisation conditions. However, for useful diagnosis it is desirable to provide a measure of existing fault severity so that an informed decision on any critical proactive action can be reliably made. This section thus proposes a diagnostic method to estimate the demagnetisation severity from the in situ flux density measurements.

The analysis of different fault levels in section V.B has demonstrated that the observed pulse shaped flux density measurement is proportional to the magnetic field of the PM arc. This is generally expected, as the level and

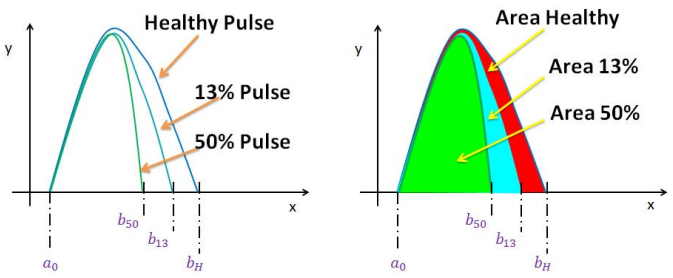

Fig. 13. Demagnetisation fault severity index calculation method.

distribution of a passing PM pole magnetisation will determine the in-situ sensor observed level and distribution of magnetostrictive strain and thus the recorded pulse characteristic, i.e. demagnetising a section of the pole arc will in relative proportion alter the recorded pulse profile. The estimation and monitoring of the pulse area could therefore provide a useful diagnostic index of demagnetisation fault severity. The fundamental idea is illustrated in Fig. 13a which represents the generalized pulse characteristics observed in healthy and 13% and 50% demagnetization fault operating conditions. A diagnostic index based on the individual pulse area value, *Area Index*, illustrated in Fig. 13b, can thus be defined as an integral of the recorded pulse shaped flux density variation:

$$Area\ Index = \int_{a_0}^{x_f} Pulse\ dx, \tag{3}$$

where: *Pulse* = recorded pulse profile, e.g. healthy pulse or 13% or 50% demagnetisation pulse in Fig. 13; $x_f = b_h$ for a healthy pulse; $x_f = b_{13}$ for 13 % pulse; $x_f = b_{50}$ for 50% pulse.

The proposed method was applied to the in-situ sensor measurements under the examined healthy and faulty conditions, calculating the single pulses area based on the definition put forward in (3). In order to mitigate the effect of pulse shape distortion at higher loads (see Fig. 12) and allow for effective determination of the reference magnetic flux density level for the integral in (3), the peaks full width half maximum at −3dB was used to define the integration limits a_0, b_h, b_{13} and b_{50} of the pulse peak.

Fig. 14. shows the integrated measurements' areas for healthy, 13 % and 50% demagnetisation fault at LS and 25% load, HS and 50% load, and FS and 100% load. The corresponding calculated *Area Index* values are shown in Fig 15: for ease of interpretation these are normalised with respect to healthy rotor *Area Index* value and presented as trends versus the health conditions status. The results demonstrated that the proposed diagnostic index enables unambiguous tracking of the rotor PMs' magnetisation level and relative quantification of the demagnetisation fault severity. For the 13 % demagnetisation case, the calculated index for the three examined operating conditions shows the occurrence of demagnetisation condition with a 6−17 % severity. In case of the 50% demagnetisation fault the index shows the occurrence of demagnetisation condition with a severity of 30−57 %. The observed error is an inherent artefact of the nature of the fault induced measurement distortion. More importantly,

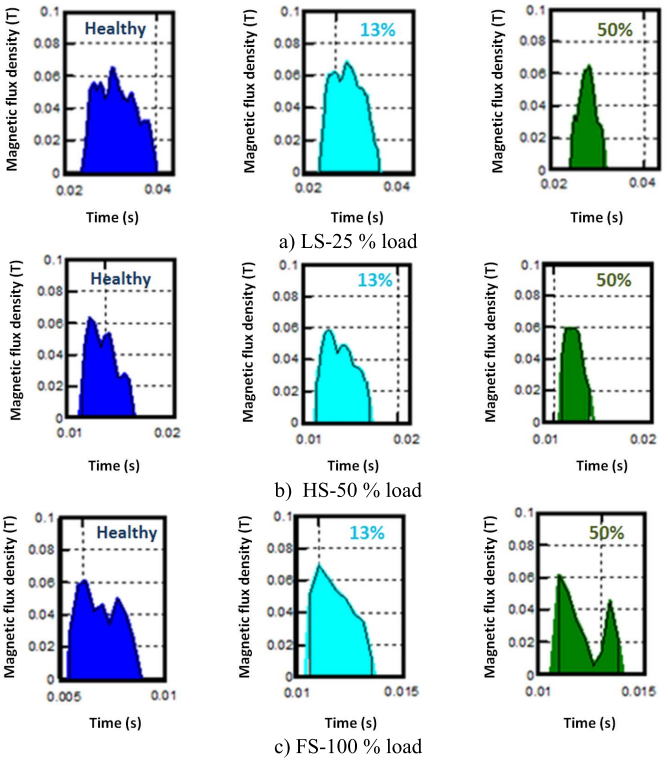

Fig. 14. Integrated areas for healthy, 13 % and 50% demagnetised rotor.

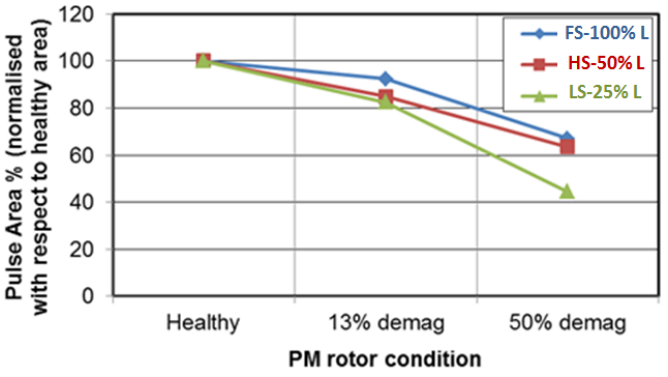

Fig. 15. Area index for fault severity diagnosis.

the presented measurements are seen to enable reliable trending of the demagnetization fault level propagation, which is valuable in practical applications.

VI. Conclusions

This paper reported an FBG magnetostrictive sensor design and application for in-situ monitoring of the rotor PMs' health condition in electrical machines. The proposed sensor design allows a relatively straightforward installation and retrofit to existing machinery, without compromising the integrity of core machine elements.

The magnetic sensor performance is validated in laboratory tests on a commercial inverter driven PM synchronous machine. It is shown that the in-situ measurements allow for effective recognition of the rotor PM magnetisation level, which is challenging to achieve with conventional machine diagnostic methods. Finally, a diagnostic index is

proposed and experimentally validated that utilizes the in-situ measurements to extract information on demagnetization severity.

The presented sensor design, implementation and utilization principles could underpin the development of improved condition monitoring and diagnostic schemes for PM electrical machinery.

REFERENCES

[1] B. Sarlioglu, C. T. Morris, D. Han, and S. Li, "Driving toward accessibility: A review of technological improvements for electric machines, power electronics, and batteries for electric and hybrid vehicles," *IEEE Ind. Appl. Mag.*, vol. 23, no. 1, pp. 14–25, Jan. 2017.

[2] A. Mohammed, J. I. Melecio, and S. Djurovic, "Open-circuit fault detection in stranded PMSM windings using embedded FBG thermal sensors," *IEEE Sensors J.*, vol. 19, no. 9, pp. 3358–3367, May 2019.

[3] S. Choi *et al.*, "Fault diagnosis techniques for permanent magnet AC machine and drives—A review of current state of the art," *IEEE Trans. Transport. Electrific.*, vol. 4, no. 2, pp. 444–463, Jun. 2018.

[4] J.-C. Urresty, J.-R. Riba, and L. Romeral, "A back-EMF based method to detect magnet failures in PMSMs," *IEEE Trans. Magn.*, vol. 49, no. 1, pp. 591–598, Jan. 2013.

[5] D. Casadei, F. Filippetti, C. Rossi, and A. Stefani, "Magnets faults characterization for permanent magnet synchronous motors," in *Proc. IEEE Int. Symp. Diag. Electric Machines, Power Electron. Drives*, Cargese, France, Aug. 2009, pp. 1–6.

[6] W. Le Roux, R. G. Harley, and T. G. Habetler, "Detecting rotor faults in low power permanent magnet synchronous machines," *IEEE Trans. Power Electron.*, vol. 22, no. 1, pp. 322–328, Jan. 2007.

[7] K. Liu and Z. Q. Zhu, "Position-offset-based parameter estimation using the Adaline NN for condition monitoring of permanent-magnet synchronous machines," *IEEE Trans. Ind. Electron.*, vol. 62, no. 4, pp. 2372–2383, Apr. 2015.

[8] T. Goktas, M. Zafarani, K. W. Lee, B. Akin, and T. Sculley, "Comprehensive analysis of magnet defect fault monitoring through leakage flux," *IEEE Trans. Magn.*, vol. 53, no. 4, pp. 1–10, Apr. 2017.

[9] Z. Yang, X. Shi, and M. Krishnamurthy, "Vibration monitoring of PM synchronous machine with partial demagnetization and inter-turn short circuit faults," in *Proc. IEEE Transp. Electrific. Conf. Expo (ITEC)*, Dearborn, MI, USA, Jun. 2014, pp. 1–6.

[10] A. Mohammed and S. Djurovic, "Stator winding internal thermal monitoring and analysis using *in situ* FBG sensing technology," *IEEE Trans. Energy Convers.*, vol. 33, no. 3, pp. 1508–1518, Sep. 2018.

[11] A. Mohammed and S. Djurovic, "*In-situ* thermal and mechanical fibre optic sensing for in-service electric machinery bearing condition monitoring," in *Proc. IEEE Int. Electr. Mach. Drives Conf. (IEMDC)*, San Diego, CA, USA, May 2019, pp. 37–43.

[12] K. M. Sousa, U. J. Dreyer, C. Martelli, and J. C. Cardozo Da Silva, "Dynamic eccentricity induced in induction motor detected by optical fiber Bragg grating strain sensors," *IEEE Sensors J.*, vol. 16, no. 12, pp. 4786–4792, Jun. 2016.

[13] M. Fabian, D. M. Hind, C. Gerada, T. Sun, and K. T. V. Grattan, "Comprehensive monitoring of electrical machine parameters using an integrated fiber Bragg grating-based sensor system," *J. Lightw. Technol.*, vol. 36, no. 4, pp. 1046–1051, Feb. 2018.

[14] J. P. V. Fracarolli *et al.*, "Development and field trial of a FBG-based magnetic sensor for large hydrogenerators," *Proc. SPIE*, vol. 9852, May 2016, Art. no. 98520L .

[15] G. Bieler and M. M. Werneck, "A magnetostrictive-fiber Bragg grating sensor for induction motor health monitoring," *Measurement*, vol. 122, pp. 117–127, Jul. 2018.

[16] J. I. Melecio, A. Mohammed, and S. Djurović, "Characterisation of FBG based magnetic field sensor response sensitivity to excitation orientation for rotating electric machine applications," in *Proc. 8th Medit. Conf. Embedded Comput. (MECO)*, Budva, Montenegro, Jun. 2019, pp. 1–5.

[17] C. Ambrosino, S. Campopiano, A. Cutolo, and A. Cusano, "Sensitivity tuning in Terfenol-D based fiber Bragg grating magnetic sensors," *IEEE Sensors J.*, vol. 8, no. 9, pp. 1519–1520, Sep. 2008.

[18] A. Mohammed and S. Djurovic, "FBG thermal sensing features for hot spot monitoring in random wound electric machine coils," *IEEE Sensors J.*, vol. 17, no. 10, pp. 3058–3067, May 2017.

[19] G. Engdahl, Ed., *Handbook of Giant Magnetostrictive Materials*. New York, NY, USA: Academic, 2000.

[20] E. Hristoforou and A. Ktena, "Magnetostriction and magnetostrictive materials for sensing applications," *J. Magn. Magn. Mater.*, vol. 316, no. 2, pp. 372–378, Sep. 2007.

[21] N. Ekreem, A. Olabi, T. Prescott, A. Rafferty, and M. Hashmi, "An overview of magnetostriction, its use and methods to measure these properties," *J. Mater. Process. Technol.*, vol. 191, nos. 1–3, pp. 96–101, Aug. 2007.

[22] (2019). *Terfenol-D Physical Properties*. [Online]. Available: http://tdvib.com/terfenol-d/

[23] Stratasys. (2019). *Dimension 1200es 3D Printer*. [Online]. Available: https://www.stratasys.com

[24] I. Juan Melecio, S. Djurovic, and N. Schofield, "An FEA model study of spectral signature patterns of PM demagnetization faults in synchronous PM machines," in *Proc. 9th IET Int. Conf. Power Electron. Mach. Drives (PEMD)*, Apr. 2018, pp. 4127–4132.

[25] J. I. Melecio, A. Mohammed, N. Schofield, and S. Djurovic, "3D-printed rapid prototype rigs for surface mounted PM rotor controlled segment magnetisation and assembly," in *Proc. IEEE Int. Electr. Mach. Drives Conf. (IEMDC)*, San Diego, CA, USA, May 2019, pp. 1830–1836.

[26] (2019). *Flux Electromagnetic Finite Element Software*. [Online]. Available: https://www.altair.com/flux/

Anees Mohammed received the M.Sc. degree in electrical power engineering from the University of Newcastle, U.K., in 2010, and the Ph.D. degree in electrical and electronic engineering from the University of Manchester, U.K., in 2019.

He is currently a Research Associate with the Power Conversion Group, University of Manchester. He spent four years working as an Assistant Lecturer with Benghazi University, Libya. His research interests are in electric machines, drives, and condition monitoring.

Juan I. Melecio received the B.S. degree in mechatronics engineering and the M.Sc. degree in energy engineering from Tecnológico de Monterrey, and the Ph.D. degree in electrical and electronic engineering from the University of Manchester, U.K., in 2019. He is currently working for Schneider Electric, Cedar Rapids, IA, USA. His current research interests include finite-element analysis, electrical machines, drives, and condition monitoring.

Siniša Djurović (Member, IEEE) received the Dipl.Ing degree in electrical engineering from the University of Montenegro, in 2002, and the Ph.D. degree in electrical and electronic engineering from the University of Manchester, in 2007.

He is currently a Senior Lecturer with the Power Conversion Group, University of Manchester. His research interests are in the area of operation, design, monitoring, and diagnostics of electric machines and drives.